Available online at www.sciencedirect.com
SCIENCE DIRECT®
Journal of Non-Crystalline Solids 334&335 (2004) 532–539
JOURNAL OF NON-CRYSTALLINE SOLIDS
www.elsevier.com/locate/jnoncrysol

Oxidation kinetics of an AlCuFeCr approximant compound: an ellipsometric study

G. Bonhomme [a,*], M. LeMieux [b], P. Weisbecker [a], V.V. Tsukruk [b], J.M. Dubois [a]

[a] Laboratoire de Science et Génie des Matériaux et de Métallurgie (UMR 7584 CNRS-INPL) Ecole des Mines, Parc de Saurupt, 54042 Nancy cedex, France
[b] Department of Materials Science & Engineering, Iowa State University, Ames, IA 50011, USA

Abstract

Using single wavelength laser ellipsometry ($\lambda = 634$ nm), we have studied the oxidation kinetics of bulk polycrystalline samples of an AlCuFeCr orthorhombic approximant compound of the decagonal phase. Up to 300 °C in dry air, nearly no evolution of the ellipsometric characteristics was detected, which can be explained assuming that the growth of the oxide layer stops shortly after beginning the exposure to temperature and air. Above this temperature, the changes of the ellipsometric characteristics pointed out a higher oxidation rate and a continuous growth of the oxide layer. In boiling water, we found that the kinetics of oxidation were as fast as when above 300 °C in dry air. Taking also into account atomic force microscopy measurements of the surface roughness, plausible scenarios for the oxidation process are inferred from our data.

PACS: 68.47.De; 61.44.Br

1. Introduction

Low surface energy and, hence, low wettability, are considered to be signatures of quasicrystals along with their high hardness and low thermal conductivity [1–6]. Measurements of the adhesion energy of water show low values, which are closer to the ones observed with low polar polymer surfaces rather than to metallic alloys [2,3]. Significant differences in surface properties were observed for quasicrystals studied in high vacuum as compared to materials with similar compositions in ambient air [7,8]. A critical role of the oxidation kinetics and thickness/composition of the oxide layers was pointed out in several recent publications [3,9,10]. Various groups have studied the oxidation of quasicrystals and related compounds. Most investigations focused on the oxidation behavior of polycrystalline compounds of the Al–Cu–Fe family (including orthorhombic O1–AlCuFeCr) [9,11,14,15] and single domain AlPdMn [12,13]. Basically, the presence of pure oxygen in contact with a freshly prepared quasicrystalline surface was shown to lead first to a significant aluminum enrichment of the surface and ultimately to the formation of a layer of amorphous alumina. By contrast, oxidation in water or humid air also results in the oxidation of the transition metals (Fe and Mn and eventually Cr) whereas the other two metals (Cu or Pd) do not take part in the oxide layer. Another study was dedicated to high temperature oxidation, i.e. from 750 to 900 °C [16,17]. Finally, a few studies concerned temperatures and atmospheres that do occur in actual or possible applications such as frying pans or selective solar absorbers [18,19].

In this study, we present the first results of the use of single wavelength ellipsometry to determine the oxidation kinetics of an AlCuFeCr orthorhombic approximant of the decagonal quasicrystal. This compound was designed for use as a coating for cooking applications [5]. The temperature in these applications ranges from 100 °C (in water or in the presence of food) to 500 °C if the cooking plate is exposed to ambient air while uncovered by water or food for roughly 30 min at full power. Thus, we investigated oxidation under these conditions.

* Corresponding author. Present address: Saint-Gobain NRDC, 9 Goddard Rd., Northboro, MA 01532, USA. Tel.: +1-508 351 7573; fax: +1-508 351 7596.
E-mail address: gaetan.bonhomme@saint-gobain.com (G. Bonhomme).

0022-3093/$ - see front matter © 2004 Elsevier B.V. All rights reserved.
doi:10.1016/j.jnoncrysol.2003.12.036

2. Experimental

Cylindrical bulk samples of 20 mm × 30 mm (20 mm being the diameter) have been uni-axially hot-pressed at 14 MPa under reduced helium pressure (750 mbar) from a batch of 25–53 μm atomized powder of $Al_{70}Cu_9Fe_{10.5}Cr_{10.5}$ (at.%, nominal composition). The cylinders were then sliced using a diamond wire saw to half or complete disks of 20 mm diameter and 3 mm thickness. All these disks, after careful polishing down to 4000 SiC grinding paper, were found to be single phase by X-ray diffraction (XRD). Some of the material was crushed in an agate mortar and investigated by transmission electron microscopy (TEM). The TEM investigation confirms that the samples are single phase and comprise the so-called O_1 phase (Bmm2), which is a 2/1 3/2 base-centered orthorhombic approximant, with $a = 23.6$ Å, $b = 12.27$ Å – the periodicity of decagonal phase – and $c = 32.5$ Å. However, because of the high degree of disorder usually observed with this compound, we do not exclude the possible presence of other minority O-phases, particularly the O_2-phase that is often detected along with the O_1 phase and forms with it a twinned microcrystalline structure (for more details about the crystalline structure and microcrystalline texture, see Refs. [20–23]). Yet, no evidence for the presence of any other crystalline phase is found by XRD. A special device was setup at Ames Laboratory to oxidize several samples for different times at the same temperature without modifying the well-controlled atmosphere when removing individual samples; a schematic is shown in Fig. 1. It consists of a 1.20 m long quartz tube, connected on one side to a cylinder of pure dry air (99.99% specified without H_2O) and on the other side to an outlet bubbling through a bath of mechanical pump oil. Therefore, samples are permanently covered by a flow of dry air set roughly at 235 ml/min. Inside the tube, the samples, shipped on alumina plates, are set regularly so that only one at a time is heated in the furnace. The whole tube holding the samples slides inside a tubular furnace. Up to four samples could be oxidized this way for different times before re-opening the sealed tube to treat a new set of samples. Before oxidation, the samples were carefully polished as follows. They were ground with SiC paper from 320 grit down to 4000 grit (European units), using only water as a lubricant. They were then ultrasonically cleaned, rinsed in methanol, and then air-dried. Visual inspection of the 4000 grit polished surface allows one to distinguish the polishing lines along one direction. Four different oxidation temperatures and up to four different atmospheres were tested. First, in the special furnace, we used dry air and 100, 200, 400 and 500 °C temperatures. These temperatures are those of the thermocouples located close to the heating element of the furnace. In the following, we refer to these samples as the T °C-dry-air series, T °C being the heat treatment temperature in °C units. The 200 °C series was also tested with pure air bubbling through deionized water before reaching the tubular furnace area, as demonstrated in Fig. 1. This series is called the 200 °C-wet-air series hereafter. At 500 °C, a series was oxidized in another furnace in ambient air (at room temperature, a humidity coefficient of up to 70% was measured). Finally, a series of samples was oxidized in

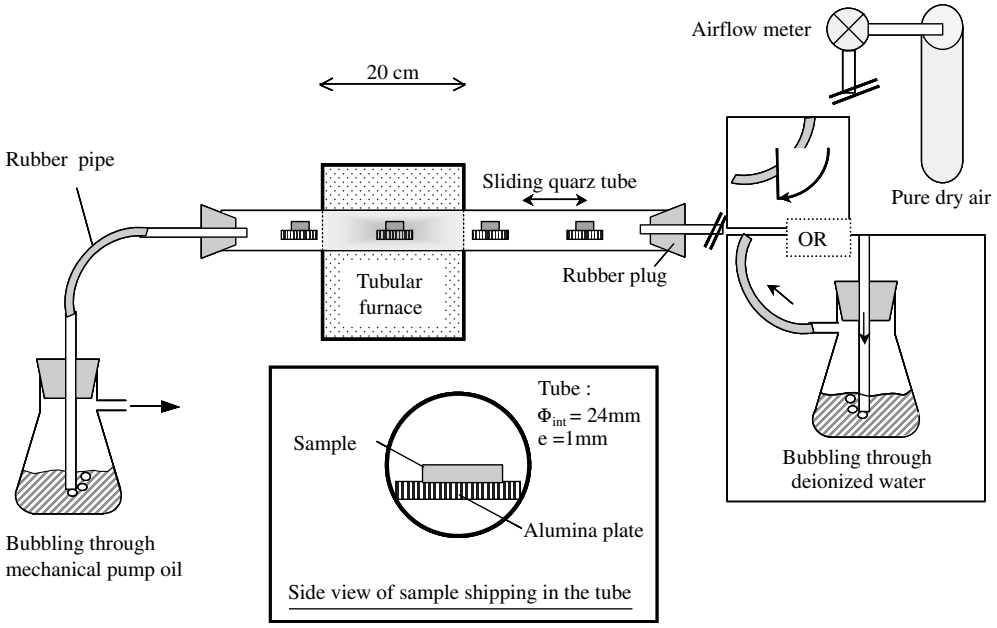

Fig. 1. Schematic diagram of the device used to oxidize the samples in dry air or in wet air.

deionized water boiling in a beaker. A total of seven series of samples, and oxidation times ranging from 1 to 4320 min were studied.

Ellipsometry is a quick, highly precise, non-destructive optical technique, which deals with the measurement and interpretation of changes in the polarization state of polarized light undergoing oblique reflection from a sample surface [24,25]. The quantities measured are the ellipsometric angles, ψ and Δ, related to the complex ratio of the Fresnel coefficients, R_p and R_s, for light polarized parallel (p) and perpendicular (s, from German Senkrecht) to the plane of incidence such that

$$R_p/R_s = \tan\psi \cdot e^{(i\Delta)},$$

R_p and R_s are defined as the ratio of the amplitude of the outgoing wave to the amplitude of the incoming wave in the direction parallel and perpendicular to the plane of incidence, respectively. Physically, Δ is the difference of the two phase shifts δ between the p-wave and s-wave before and after reflection ($\Delta = (\delta(p-s)_{\text{before}} - \delta(p-s)_{\text{after}})$). Its value can range from 0 to 360°; $\tan\psi$ is the ratio of the amplitude of the total reflection coefficients, and the value of ψ ranges from 0 to 90 °. The amount of ellipticity that is induced by reflection depends on the surface. It mostly relies on the optical constants of both substrate and possible overlayers, known as the complex index of refraction $N = n - ik$ ($n = c/v$ being the usual index of refraction which, for dielectric materials, is an inverse measure of the velocity of light v in the material, related to the speed of light in free space c, and k the coefficient of extinction that measures how rapidly intensity decreases as light passes through the material). The ellipticity also depends on the thickness of the overlayers, their roughness, etc.

The optical device used was a Discrete Polarization Modulation Compell Ellipsometer (InOmTech, Inc.). It consists of a single wavelength laser source (AlGaInP red diode, wavelength $\lambda = 634$ nm.) linearly polarized with sequentially switched orthogonal polarizations. The polarizer and analyzer are anisotropic calcite wedges, and the detectors are two Si photodiodes. The analyzed area is $\cong 1$ mm^2. The incidence angle was set to 70° to maximize the reflection parameters. The values of Δ and ψ are averaged over 10s time intervals with one acquisition every 0.3 s, which makes 30 measurement statistics for each value. For each sample, ψ and Δ were measured at 3–5 locations (5 most of the time) for each orientation, the plane of incidence of the laser beam being set along the polishing lines and perpendicular to them. The precision of the device is very good, $\delta\Delta = \pm 0.05°$ and $\delta\psi = \pm 0.005°$.

High–resolution surface topography and phase imaging was studied with an atomic force microscope (AFM), Dimension 3000 (Digital Instruments). The instrument is installed on a vibration damping isolation table and is protected by an acoustic blocking hood. Measurements were made in the tapping mode according to the usual procedures described elsewhere [26,27]. The tip was V-shaped silicon coated with silicon nitride (Si_3N_4) for wear protection. The tip radius was measured with size-calibrated gold nanoparticles before (12–20 nm) and after scanning (30 nm), and the same tip was used for all measurements. The surface microroughness was calculated as the Root Mean Square (RMS) parameter after a flattening procedure.

3. Results

Fig. 2 presents all of data point acquired by ellipsometry for the seven series of samples. A standard presentation is used in the $\{\psi, \Delta\}$ plane. Oxidation at $t = 0$ s consists of the native oxide grown during the surface preparation of the sample. As pointed out before [9,11,12], because we are using water to polish the samples, the native oxide layer at $t = 0$ will be mainly composed of amorphous aluminum oxide, plus Fe and Cr as their respective oxides or as cations inside the alumina amorphous structure. The average values of the ellipsometric angles at $t = 0$ are $\Delta = 143 \pm 1°$ and $\psi = 26.9 \pm 0.5°$. Note that at this experimental wavelength (634 nm) these values are between those of semiconductors and metals [25]. As easily noticed from Fig. 2, all data points follow the same general trend: with increasing oxidation time, Δ keeps decreasing and ψ keeps increasing, in an elliptic way. This evolution of the parameters corresponds well to the growth of an oxide layer on a metallic substrate [24,25]. Moreover, in all cases except the 100 °C-water series, the points of all series follow exactly the same path and can not be distinguished as can be seen in the figure. Hence, these growing oxide layers have all the same optical properties and growth specificities, meaning that the only possible differences concern kinetics (i.e. thickness) and not the nature of the oxide. This does not mean that both do not change, but if they do evolve with increasing oxidation time, it is in the same way for all series. For the 100 °C-water series, the behavior is clearly that of a growing oxide also, but the data points do not follow the same path: they are shifted to higher values of ψ. This means that the evolution of the oxide thickness and/or its shape (presumably both) is different under this oxidation condition. Because of the environment used, this latter case certainly leads to complex corrosion products, such as hydroxides and hydrogenated spinels, involving all chemical species. Visual (or optical microscopy) inspection of the oxidized surface confirms that changes are more pronounced with the 100° C-water series: even for the longest times, no changes are detected for the other series whereas iridescent blue–yellow spots ranging from less than 1 mm up to 2–3 mm in diameter are seen at the surface of the 100 °C-water series samples.

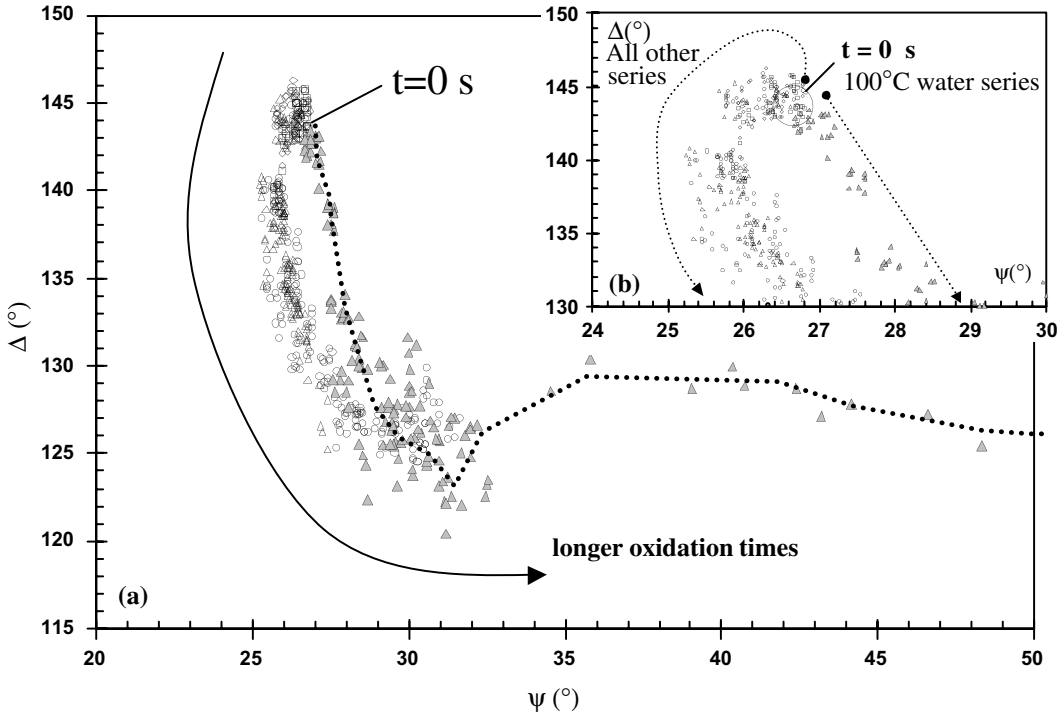

Fig. 2. (Δ, ψ) charts of all the data points of all series (a) and enlargement of the data in the range $24 \leqslant \psi \leqslant 30°$ (b). Note the general trend followed by all series of samples except the 100 °C-water series shown by gray triangles (the dashed line is only a guide for the eye).

There are also differences in the area they occupy in the $\{\psi, \Delta\}$ plan, as demonstrated in Fig. 3(c) (the data points located here appear to be the ones for the very first minutes of oxidation for 400, 500 °C-dry air and 100 °C-water series whereas all points of the 100 and 200 °C series are contained in this area). All the data points make a loop around the starting point at $t = 0$, before following the usual growing oxide behavior, whereas the 100 °C-water series just exhibits the usual behavior immediately after beginning the oxidation experiment, with Δ and ψ respectively decreasing and increasing with time. The origin of this loop is not yet clearly explained. Furthermore, we checked that aligning the plane of incidence of the laser beam either perpendicular or parallel to the polishing lines did not change significantly Δ and ψ values: the orientation perpendicular to the lines results into values that are systematically shifted towards ψ values lower by approximately $-0.3°$.

A convenient way to represent changes in the ψ and Δ parameters versus time for the different series is to plot the sum of the absolute values of the differences between any couple of ψ_i and Δ_i at $t = t_i$ and ψ_0 and Δ_0 at $t = 0$, namely $y(t_i) = (|\Delta_i - \Delta_0| + |\psi_i - \psi_0|)$. This change is clearly related for all series (with some precautions for the 100 °C-water series) to the increasing thickness of the growing oxide, as demonstrated before in this paper. Fig. 3 presents such a plot of $y(t)$ as a function of oxidation time t. Each data point in the figure is the arithmetic average of 6–10 data points (3–5 points at different locations, along and across the polishing lines) on the oxidized surface at a certain time. The standard deviations σ are very important, $\sigma(\Delta) = 1°$ and $\sigma(\psi) = 0.5°$. For clarity, these deviations are represented only for two series, which indicates that a change of $y(t)$ by 3° can hardly be related to any change of the oxide layer thickness. From this figure however, different growth kinetics can be deduced as follows. There is nearly no evolution of the parameters for the 100 °C-dry-air as well as for the 200 °C-dry-air and 200 °C-humid-air series. For the three other series, the kinetics follows this order: oxidation at 400 °C in dry air is slower than at 500 °C in ambient air, which itself is slower than at 500 °C in dry air. The two latter kinetics are not what one would expect, but show the high sensitivity of the surface oxidation to temperature. As described before, two different furnaces were used for our oxidation experiments and it may have occurred that the temperature in the ambient air furnace was below that in the other furnace. Concerning kinetics, Fig. 3(a), one could deduce that oxidation stops after roughly 1200 min because there is no significant evolution of the Δ and ψ angles beyond that point. Fig. 3(b) shows the time scale in a logarithmic way, which points out that diffusion of the species through the substrate and oxide layer follows non-linear kinetics. We intentionally did not

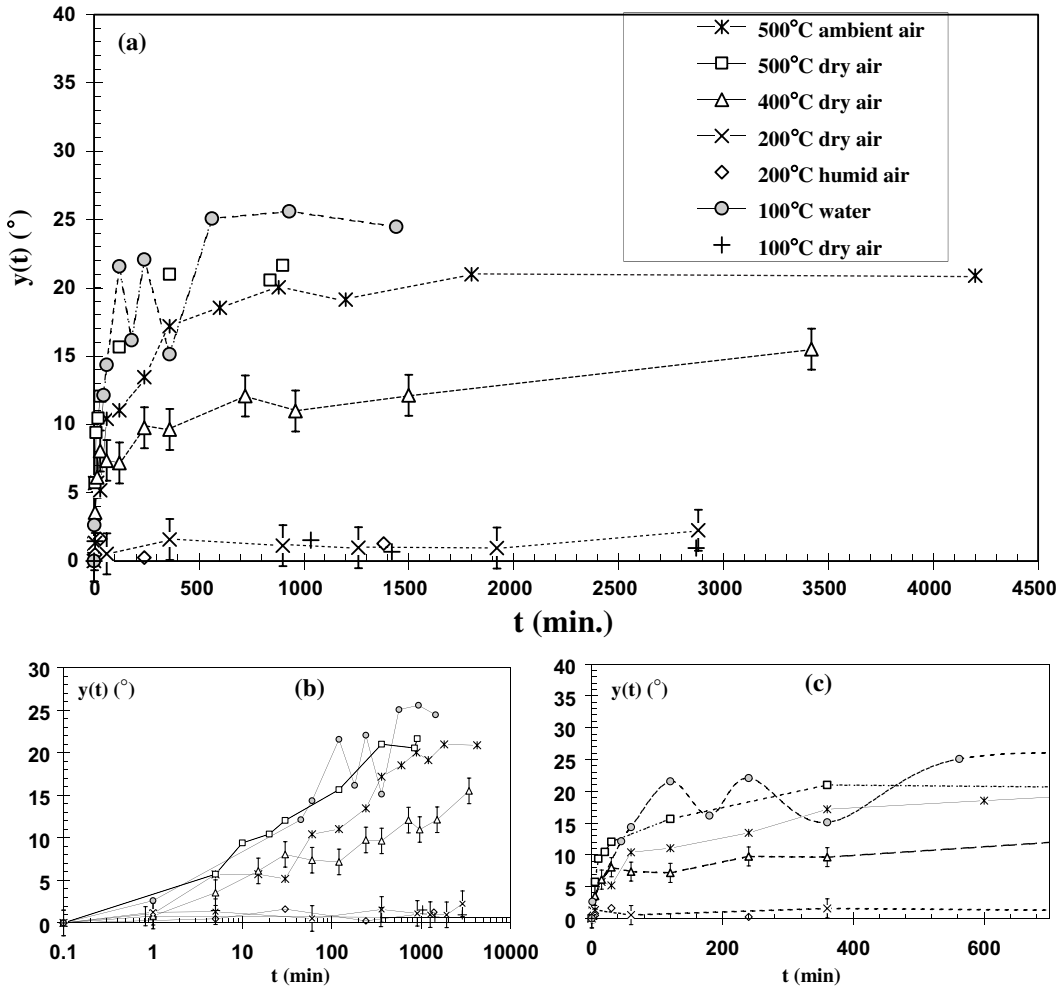

Fig. 3. Plot of $y(t) = (|\Delta_i - \Delta_0| + |\psi_i - \psi_0|)$ versus oxidation time. A general view is displayed in (a), details for short oxidation times in (b), and oxidation times are displayed in a logarithmic scale in (c). Symbols used for the various sample series are the same in (a), (b) and (c) and are indicated in (a). Lines are drawn only to guide the eye.

plot the time scale following the usual oxidation kinetics laws (parabolic, logarithmic or inverse logarithmic, see for instance [35,36]) because the $y(t)$ values are not linearly related to thickness: the equations depend on the model used to fit the data. This point will be discussed later. Finally, assuming that the oxide dielectric constant and its geometry are the only parameters that lead to the observed systematic $\Delta\psi$ shift, as discussed before, the kinetics data extracted from the 100 °C-water series would be comparable to the ones obtained from the 500 °C-dry-air series.

To understand better the nature of the surface changes during oxidation, we have performed AFM measurements on different samples. Topographical AFM views of different surfaces are shown in Fig. 4(a), (b) and (c). To clearly identify the changes, a sample was polished with diamond paste and water lubricant down to a 0.25 μm grinding particle size and then scanned. The result is shown in Fig. 4(a). The same sample was then oxidized in ambient air at 500 °C for 4320 min, and scanned again (Fig. 4(b)). The most oxidized sample, after 4200 min at 500 °C in ambient air, is shown in Fig. 4(c). One should be aware of the scale distortions on these figures: the magnification along depth is 1000 times larger than along the lateral distances. All surfaces are very flat, exhibiting visually a mirror-like structure, and the angle between a horizontal line and an oblique line of a groove in Fig. 4(c) is far below 1° (instead of nearly 90° as seen in the figure).

Comparing Fig. 4(a) and (b), the difference between a sample at room temperature and an oxidized one appears in the form of needle shaped oxide bumps (because of vertical exaggeration, the real inclination angle being close to 2°), roughly 25–30 nm in height and distributed all along the oxidized surface. Because these peaks, that are clearly identifiable and periodically spaced, occupy a minor fraction of the whole surface, the RMS roughness measured by AFM does not vary significantly with oxidation, being 0.8 nm for the room temperature sample, and 1.5 nm for the

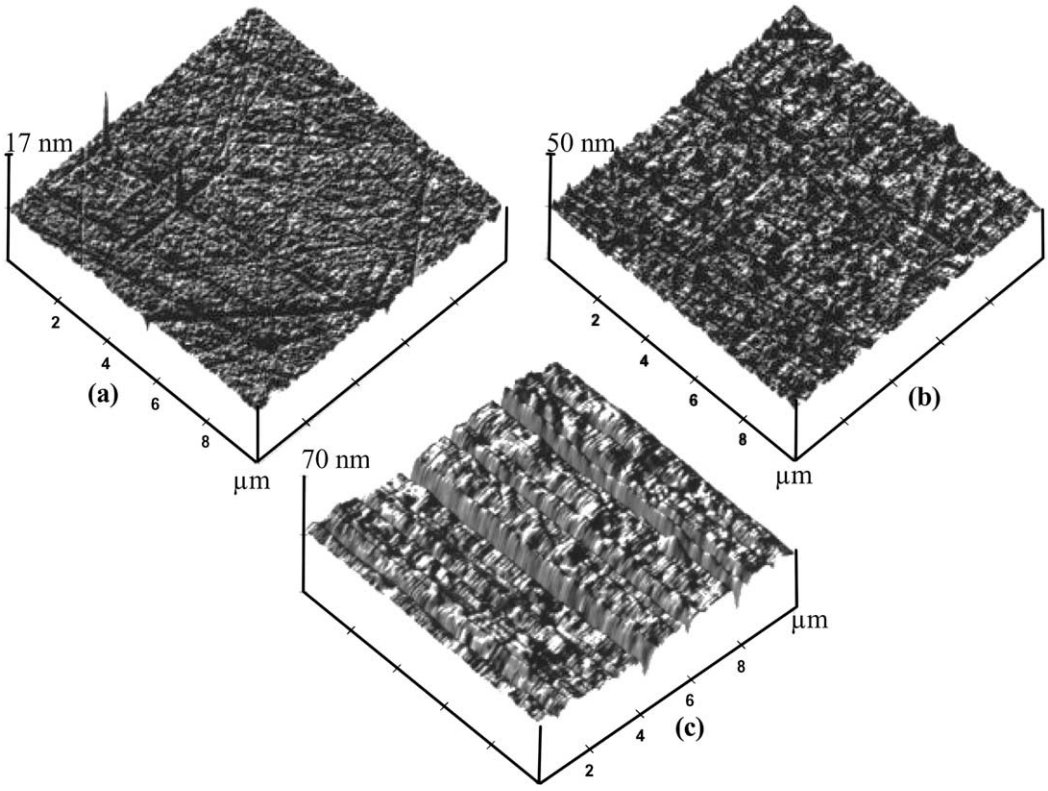

Fig. 4. Surface topographical AFM views of a sample polished with diamond paste (0.25 μm) and left at room temperature (a), after oxidation for 72 h at 500 °C in ambient air (b) and after oxidation for 70 h at 500 °C in ambient air (c). Note the differences between the three vertical length scales, and between the vertical and horizontal length scales.

oxidized one. These peaks almost completely blur the initial polishing lines (5 nm in height). The opposite behavior is seen in Fig. 4(c) with the sample polished with 4000 SiC grinding paper. The polishing lines, making a very large nanometric roughness (+70 nm), are clearly visible whereas the 25 nm sharp peaks are hardly recognizable. The overall RMS roughness was calculated to be 7 nm, but it can be split into a component of RMS roughness equal to 2 nm parallel to the polishing lines (roughly equal to the plane roughness of the very well polished oxidized sample) and a perpendicular component with RMS roughness of 11 nm. Finally, grazing incidence XRD (GIXRD) was performed on the surface of the oxidized samples. No trace of crystalline oxides was found, nor any decomposition of the orthorhombic approximant into other crystalline phases that would sign any significant depletion in aluminum at the surface of the substrate close to the metal/oxide interface.

4. Discussion

The first point worth of discussing is the fits of the data by different models. Using several routines, we tried to fit our data and concluded that it cannot be fit with any of the following models:

(1) An optically isotropic and homogeneous flat substrate, with fixed n and k indexes, with one or several optically isotropic and homogeneous flat oxide layers with fixed refractive indexes on-bp [24,25,28].
(2) Model (1) with complex optical indexes of refraction for both the substrate and overlayer(s) that vary with oxidation time (thus changing the reflecting surface composition).
(3) Model (1), taking into account the initial roughness using effective-medium equations, which consist of replacing the roughness between two layers (one might be ambient air) by a new flat layer, the thickness and indexes of which depend on the model used [24,25,28–31].
(4) Models (1), (2) and (3) taken together with progressive changes in the roughness reflecting AFM measurements.

When trying to apply these models, several difficulties arose. First, at this particular wavelength, no accurate measurements of the n and k indexes are known for quasicrystals. Studies by Demange et al. and Eisenhammer et al. [32,33] use spectroscopic ellipsometry,

which does not give accurate measurements at single wavelengths. Moreover, in the models they used to fit the data and extract optical indexes, the native oxide layer was not included. We performed our own spectroscopic measurements, leading to data that span an interval of 3–8 for n and 2–5 for k (which is not accurate enough). Furthermore, the assumption that the n and k indexes of our oxide layers are very close to those of crystalline alumina ($n = 1.766$, $k = 0$ [34]) does not yield satisfactory results. This is because we polished our sample using water, which leads to the formation of an amorphous layer that furthermore may contain a small quantity of transition metal cations. Therefore, the n and k indexes of the oxide are also unknown parameters. And last, the way we introduced the roughness and its evolution is certainly too simplistic.

Fig. 5 shows, nevertheless, an attempt to calculate the (Δ, ψ) chart using model 1 for a series of oxide layers with thickness increasing from 3 to 18 nm by steps of 1.5 nm. The most general trends are reproduced, although imperfectly, and the order of magnitude of the thickness agrees with results from previous studies [9,11,12,14]. The main details that can not be fitted are the loop at the beginning of the curve, (yet, Graat et al. [28] showed it could be related to a change in roughness of the oxide-air interface) as well as the exact curvature and the shape of the data tail. Therefore it is hazardous to extract even a relative thickness so as to deduce valuable kinetics data, mainly for very short and very long oxidation times where the deviation from our model and the elliptic behavior is quite important.

Another point we want to discuss is the observed very high values of the standard deviations $\sigma(\Delta) = 1°$ and $\sigma(\psi) = 0.5°$ as compared to the instrumental precision, $\delta\Delta = 0.05°$ and $\delta\psi = \pm 0.005°$. This suggests that the samples are not homogeneous at the size of the incident beam ($\cong$1 mm^2). This is especially true for the 100 °C-water series for which visual inspection revealed inhomogeneities (the iridescent dots) largely exceeding the area of 1 mm^2. In the other samples, the size of the possible defects, as seen before, is only accessible through AFM (or nanoscale microscopies). No special feature was detected with standard profilometry. The samples seemed homogeneous at the accessible AFM scan size (up to 100×100 μm^2 area), and a scanning electron microscopy (SEM) examination used to probe more extended areas did not reveal any particular morphologies that would make the surface inhomogeneous at the scale of the ellipsometric range. Moreover, suspecting that such inhomogeneities grow with increasing oxidation times, we plotted the evolution of the standard deviations versus time, and found no particular change. This means that these defects are present prior to the oxidation experiment and may form during preparation or subsequent storage of the samples.

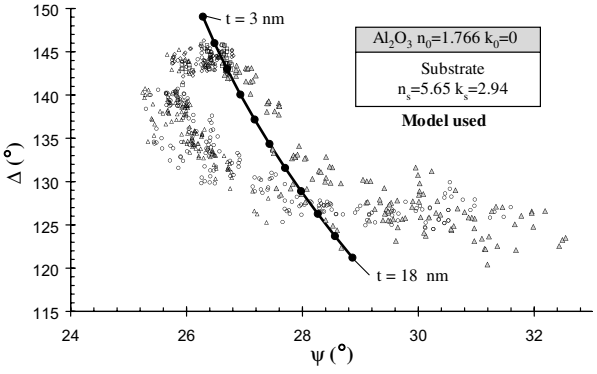

Fig. 5. Sketch of the model used to mimic the ellipsometric data. Dots on the line correspond to a successive oxide thickness ranging from 3 to 18 nm in steps of 1.5 nm.

5. Conclusion

The oxidation behavior and kinetics of an AlCuFeCr orthorhombic approximant of the decagonal phase have been studied in function of temperature, from ambient to 500 °C, and humidity, from dry air to boiling water. The following scenario of the oxidation process can be inferred from our data. Before oxidation, the oxide layer resulting from sample preparation consists of an amorphous alumina layer that may contain small quantities of transition metals cations and is approximately 4–5 nm thick [11]. Then, when the oxidation temperature is below 500 °C, and under either dry or ambient air oxidation conditions (up to 70% humidity)are used, the oxide layer will still be amorphous. The kinetics mostly rely on temperature and not much on the partial pressure of water. They are null or very sluggish below 200 °C, and activate above 300 °C. The oxide does not grow uniformly, but tends to form little islands, thus creating a nano-sized roughness. After 70 h at 500 °C, the thickness of the oxide layer reaches 20–25 nm. By contrast, the oxidation at 100 °C in boiling water is rather different, and should be dealt with considering also corrosion phenomena. The oxidation kinetics are very fast, like or even faster than the one observed at 500 °C in air.

Non-homogeneous oxidation and growing oxide layers covering the approximant phase will certainly affect the physical properties of the surface, including friction and wetting. The latter was recently assessed [37]. Ellipsometry is useful for studying the oxidation behavior, but further data on oxide free surfaces and optical properties of complex oxide layers as well as improved optical models are needed to achieve kinetics determinations.

Acknowledgements

One of us (G.B.) gratefully acknowledges P.A. Thiel and A.I. Goldmann for useful discussions and hospi-

tality at Ames Laboratory. We acknowledge A.J. Thom for setting up the special oxidation device, P. Graat, G. Guillemot, A. Sidorenko who provided most of the ellipsometric routine basis, F. Machizaud and V. Demange for the spectroscopic measurements and optical index fitting calculations, and D.J. Sordelet for his interest and support of this work. M.L. was supported by the United States Department of Energy (USDOE), Office of Science (OS), and Office of Basic Energy Science (BES), through Iowa State University under contract W-7405-ENG-82. Financial support offered by CNRS under PICS no. 545 and by Saint Gobain CREE and INPL-Nancy under ERT 'Quasicristaux Industriels' are gratefully acknowledged.

References

[1] J.M. Dubois, Phys. Scripta T 49A (1993) 17.
[2] J.M. Dubois, S.S. Kang, P. Archambault, B. Colleret, J. Mater. Res. 8 (1) (1993) 38.
[3] N. Rivier, J. Non-Cryst. Solids 153 & 154 (1993) 458.
[4] J.M. Dubois, Mat. Sci. Eng. A 294–296 (2000) 4.
[5] J.M. Dubois, A. Proner, B. Bucaille, P. Cathonnet, C. Dong, V. Richard, A. Pianelli, Y. Massiani, S. Ait-Yaazza, E. Belin-Ferré, Ann. Chim. Fr. 19 (1994) 3.
[6] C.I. Lang, D.J. Sordelet, M.F. Besser, D. Shechtman, F.S. Biancaniello, E.J. Gonzalez, J. Mater. Res. 15 (9) (2000) 1894.
[7] J.S. Ko, A.J. Gellman, T.A. Lograsso, C.J. Jenks, P.A. Thiel, Surf. Sci. 423 (2–3) (1999) 243.
[8] B. Wolf, S. Baunack, P. Paufler, Phys. Stat. Sol. A 172 (2) (1999) 317.
[9] P.J. Pinhero, J.W. Anderegg, D.J. Sordelet, M.F. Besser, P.A. Thiel, Philos. Mag. B 79 (1) (1999) 91.
[10] P. Ebert, F. Kluge, B. Grushko, K. Urban, Phys. Rev. B 60 (2) (1999) 874.
[11] P.J. Pinhero, D.J. Sordelet, J.W. Anderegg, P. Brunet, J.M. Dubois, P.A. Thiel, Mat. Res. Soc. Symp. Proc. 553 (1999) 263.
[12] P.J. Pinhero, S.L. Chang, J.W. Anderegg, P.A. Thiel, Philos. Mag. B 75 (2) (1997) 271.
[13] S.L. Chang, W.B. Chin, C.M. Zhang, C.J. Jenks, P.A. Thiel, Surf. Sci. 337 (1995) 135.
[14] M. Gil-Gavatz, D. Rouxel, P. Pigeat, B. Weber, Philos. Mag. A 80 (9) (2000) 2083.
[15] C.J. Jenks, Mater. Res. Soc. Symp. Proc. 553 (1999) 219.
[16] B.I. Wehner, U. Köster, A. Rüdiger, C. Pieper, D.J. Sordelet, Mater. Sci. Eng. A 294–296 (2000) 830.
[17] B.I. Wehner, U. Köster, Oxid. Met. 54 (5–6) (2000) 445.
[18] D.J. Sordelet, L.A. Gunderman, M.F. Besser, A.B. Akinc, in: A.I. Goldman, D.J. Sordelet, P.A. Thiel, J.M. Dubois (Eds.), New Horizons in Quasicrystals, World Scientific, Singapore, 1996, p. 296.
[19] A. Haugeneder, T. Eisenhammer, A. Mahr, J. Schneider, W. Wendel, Thin Solid Films 307 (1997) 120.
[20] C. Dong, J.M. Dubois, S.S. Kang, M. Audier, Philos. Mag. B 65 (1) (1992) 107.
[21] C. Dong, J.M. Dubois, J. Mater. Sci. 26 (1991) 1647.
[22] X.Z. Li, C. Dong, J.M. Dubois, J. Appl. Crystallogr 28 (1995) 96.
[23] W. Liu, U. Köster, F. Müller, D.M. Rosenberg, Phys. Stat. Sol. A 132 (1992) 17.
[24] R.M.A. Azzam, N.M. Bashara, Ellipsometry and Polarized Light, North-Holland, Amsterdam, 1977.
[25] H.G. Tompkins, A User's Guide to Ellipsometry, Academic, New York, 1993.
[26] B. Ratner, V.V. Tsukruk, ACS Symp. Series (1998) 694.
[27] V.V. Tsukruk, Rubber Chem. Techn. 70 (3) (1997) 430.
[28] P.C.J. Graat, M.A.J. Somers, E.J. Mittemeijer, Thins Solid Films 340 (1999) 87.
[29] D.E. Aspnes, J.B. Theeten, F. Hottier, Phys. Rev. B 20 (8) (1979) 3292.
[30] C.A. Fenstermaker, F.L. McCrackin, Surf. Sci. 16 (1969) 85.
[31] J.P. Marton, E.C. Chan, J. Appl. Phys. 45 (11) (1974) 5008.
[32] V. Demange, A. Milandri, M.C. de Weerd, F. Machizaud, G. Jeandel, J.M. Dubois, Phys. Rev. B 65 (2002) 144205.
[33] T. Eisenhammer, A. Mahr, A. Haugeneder, T. Reichelt, W.Assman, in: C. Janot, R. Mosseri (Eds.), Proceedings of the 5th International Conference on Quasicrystals, World Scientific, Singapore, 1995, p. 758.
[34] E.D. Palik, Handbook of Optical Constants of Solids, Academic, New York, 1985.
[35] F.P. Felhner, N.F. Mott, Oxid. Metals 2 (1) (1970) 59.
[36] A.F. Beck, M.A. Heine, E.J. Caule, M.J. Pryor, Corr. Sci. 7 (1967) 1.
[37] J.M. Dubois, V. Demange, G. Bonhomme, V. Fournée, D.J. Sordelet, P.A. Thiel, E. Belin-Ferré, Phys. Rev. Lett., submitted for publication.